Check for updates

doi:10.1111/evo.14318

Rugged relief and climate promote isolation and divergence between two neotropical cold-associated birds

Fábio Raposo do Amaral,[1,2] Gregory Thom,[3] Matheus S. Lima-Ribeiro,[4] Diego F. Alvarado-Serrano,[5] Julia A. C. Montesanti,[1] Katia C. M. Pellegrino,[1] Cristina Y. Miyaki,[6] Michael J. Hickerson,[7] and Marcos Maldonado-Coelho[1,8]

[1]*Departamento de Ecologia e Biologia Evolutiva, Universidade Federal de São Paulo, Rua Professor Artur Riedel, 275, Diadema, SP, 09972-270, Brazil*

[2]*E-mail: fabioraposo@gmail.com*

[3]*Department of Ornithology, Division of Vertebrate Zoology, American Museum of Natural History, Central Park West at 79th Street, New York, NY, 10024–5192, USA*

[4]*Departamento de Ciências Biológicas, Universidade Federal de Jataí, CP 03, Jataí, GO, 75804-020, Brazil*

[5]*Department of Biological Sciences, Ohio Center for Ecology and Evolutionary Studies, Ohio University, Life Sciences Building R219, Athens, OH 45701, USA*

[6]*Departamento de Genética e Biologia Evolutiva, Universidade de São Paulo, Rua do Matão, 277, Cidade Universitária, São Paulo, SP, 05508-090, Brazil*

[7]*Department of Biology, City College of New York, 160, Convent Avenue, New York, NY 10031, USA*

[8]*Department of Biology, Lund University, Lund SE-223 62, Sweden*

Received November 21, 2020
Accepted July 19, 2021

The role of historical factors in establishing patterns of diversity in tropical mountains is of interest to understand the buildup of megadiverse biotas. In these regions, the historical processes of range fragmentation and contraction followed by dispersal are thought to be mediated by the interplay between rugged relief (complex topography) and climate fluctuations and likely explain most of the dynamics of diversification in plants and animals. Although empirical studies addressing the interaction between climate and topography have provided invaluable insights into population divergence and speciation patterns in tropical montane organisms, a more detailed and robust test of such processes in an explicit spatio-temporal framework is still lacking. Consequently, our ability to gain insights into historical range shifts over time and the genomic footprint left by them is limited. Here, we used niche modeling and subgenomic population-level datasets to explore the evolution of two species of warbling finches (genus *Microspingus*) disjunctly distributed across the Montane Atlantic Forest, a Neotropical region with complex geological and environmental histories. Population structure inferences suggest a scenario of three genetically differentiated populations, which are congruent with both geography and phenotypic variation. Demographic simulations support asynchronous isolation of these populations as recently as ~40,000 years ago, relatively stable population sizes over recent time, and past gene flow subsequent to divergence. Throughout the last 800,000 years, niche models predicted extensive expansion into lowland areas with increasing overlap of species distributions during glacial periods, with prominent retractions and isolation into higher altitudes during interglacials, which are in line with signs of introgression of currently isolated populations. These results support a dual role of cyclical climatic changes: population divergence and persistence in mountain tops during warm periods followed by periods of expansion and admixture in lower elevations during cold periods. Our results underscore the role of the interplay between landscape and climate as an important mechanism in the evolution of the Neotropical montane biota.

KEY WORDS: Pleistocene, range shifts, sky islands, speciation, tropical mountains.

© 2021 The Authors. *Evolution* © 2021 The Society for the Study of Evolution.

EVOLUTION
INTERNATIONAL JOURNAL OF ORGANIC EVOLUTION

Understanding the evolutionary and ecological mechanisms responsible for the build-up of species diversity is a central theme in evolutionary biology. This is especially relevant in tropical mountains, where biotic diversity is among the highest in the world; yet only a few detailed large-scale studies have been performed to infer processes fostering population divergence and speciation in these mountains (Fjeldså et al., 2012, Flantua et al., 2019; Rahbek et al., 2019). In these regions, the historical fragmentation and contraction of habitats and subsequent dispersal mediated by rugged relief and climate fluctuations are thought to be key factors underlying the dynamics of diversification (Mayr and Diamond, 1976; Patton and Smith, 1992; Graham et al., 2014; Antonelli, 2015; Rangel et al., 2018). While empirical evidence addressing the interplay between climate and topography has been available for some time and has provided invaluable insights into the diversification of tropical montane organisms (Van der Hammen, 1961; Hooghiemstra and Van der Hammen, 2004; Chesser, 2000; Pérez-Emán, 2005; Bonaccorso, 2009; Weir, 2009; Gutiérrez-Pinto et al., 2012; Ramírez-Barahona and Eguiarte, 2013; Valderrama et al., 2014; Winger and Bates, 2015; Manthey et al. 2017, Cadena et al., 2019, Muellner-Riehl 2019, Rahbek et al., 2019), our ability to understand these range shifts in the recent and more distant past and the genomic footprint left by them is still limited. This is because these processes have rarely been empirically investigated in a detailed explicit spatio-temporal framework. In fact, conceptual and simulation models predict that actual effects of altitudinal range shifts on population differentiation represent a protracted process, suggesting mountains act as evolutionary arenas over recent- and deep-time scales (Hooghiemstra and Van der Hammen, 2004; Ramírez-Barahona and Eguiarte, 2013; Flantua and Hooghiemstra, 2018; Antonelli et al., 2018; Rangel et al., 2018; Muellner-Riehl, 2019; Rahbek et al., 2019).

If climate and topography synergistically shaped the demography and divergence of montane organisms over a long-standing rugged landscape through time, for cold-associated organisms, one would expect cycles of range contraction-divergence to have occurred in highland areas during interglacials followed by population expansion-admixture in lower elevations during glacial periods (McCormack et al., 2009; Ramírez-Barahona and Eguiarte, 2013; Flantua and Hooghiemstra, 2018, Rahbek et al. 2019). This is expected under the scenarios of strong thermal zonation that are observed in tropical regions, thereby selecting montane organisms with narrow temperature tolerances (Janzen, 1967; Patton and Smith, 1992; Moritz et al., 2000; Kozak and Wiens, 2007; Cadena et al., 2012, but see Ghalambor et al., 2006). Under this scenario, tropical montane organisms are expected to track their climatic niches by shifting their geographic ranges altitudinally over time (Wiens, 2004; Flantua and Hooghiemstra, 2018). Alternatively, organisms may not follow this expectation if they are less specialized to temperature stratification along elevation gradients or are more affected by other processes such as interspecific competition (Freeman et al., 2016). Under the latter scenario, range dynamics should be largely independent of the interplay between climate and topography, and regions of geographic isolation and secondary contact across geography and time would be random with respect to variation in temperature and elevation.

Herein, we provide evidence of the interaction between climate and topography as a driver of population differentiation for a system involving Neotropical montane birds. To this end, we take advantage of the biogeographic setting found in the Montane Atlantic Forest (hereafter MAF) that stretches along the eastern coast of South America. MAF organisms that show phenotypic differentiation coinciding with montane habitat discontinuity are especially interesting study systems, as this pattern presumably reflects genome-wide divergence resulting from an interplay between climate, topography, and the evolutionary outcomes of drift, selection, and gene flow. Here, we used an integrative approach involving coalescent-based methods applied to population-level sub-genomic datasets and paleo-distribution modeling in combination with additive regression models to test whether the interplay between Pleistocene climate changes and topography underlies patterns of divergence, genetic diversity, and the range distribution of two cold-associated sister species (Amaral et al., 2015): the Gray-Throated Warbling Finch (*Microspingus cabanisi*) and the Buff-Throated Warbling Finch (*Microspingus lateralis*). We contrasted both the fit of alternative genetic demographic and climatic suitability models to scenarios of current and past MAF configurations.

The combined distributions of these two species cover most of the MAF, where the northern *M. lateralis* inhabits highland areas above 900 m of two isolated mountain ranges in SE Brazil, the Mantiqueira and the northern portion of the Serra do Mar. This species also occurs in the Caparaó highlands, an isolated northernmost massif of the Mantiqueira mountain range (Figure 1). The southern *M. cabanisi* occurs in the southern portion of Serra do Mar and in the Serra Geral mountain range, mostly above 900 m. It is also found in lower elevation areas towards its southern limit, which includes areas in Brazil, Argentina, Paraguay, and all over Uruguay (Assis et al., 2007). These two species differ phenotypically in both plumage and vocalizations (Assis et al., 2007) and are currently separated by lower elevation forest habitats (Figure 1, Supplementary Information). Our results support a dual role of cyclical climatic changes, by which populations diverged in higher elevations followed by periods of expansion and admixture in lower elevations during cold periods of the late Pleistocene. These processes of population fragmentation and connectivity were, however, notably complex, with asynchronous divergence and connectivity across distinct mountain ranges.

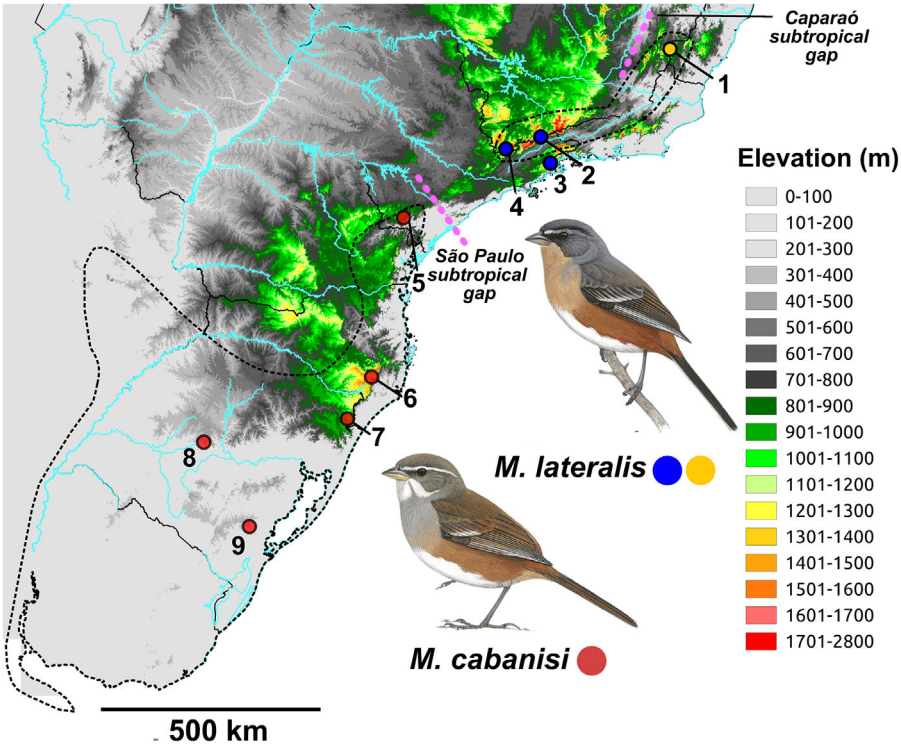

Figure 1. Localities sampled. Blue and yellow circles represent *Microspingus lateralis* while red circles represent *Microspingus cabanisi*. Major highlands include Caparaó (1), Northern Serra do Mar (3), Mantiqueira (2 and 4), Southern Serra do Mar (5), and Serra Geral (6 and 7), while lowlands include two localities (8 and 9). Two lower elevation regions that mark phenotypic and/or genotypic shifts, named here Caparaó and São Paulo subtropical gaps are indicated by pink dashed lines. See Supporting Information and Table S1 for details on samples, and coordinates. Plates reproduced from Jaramillo 2020a and Jaramillo 2020b.

Methods

GEOLOGICAL AND ENVIRONMENTAL HISTORY OF MAF

The tectonic processes that originated in the eastern Brazilian highlands as well as their ages are still a matter of debate. The major uplift events were suggested to have started during the lower Cretaceous (ca. 120 million years ago) as a consequence of the Gondwana land breakup (Melo et al., 1985; Franco-Magalhães et al., 2014). Alternatively, the uplift is proposed to have resulted from the three main pulses of Andean orogeny, with the early ages of the mountain ranges (i.e., Serra do Mar) estimated to be ca. 90 million years ago (Meisling et al., 2001; Karl et al., 2013). Additionally, a range of evidence indicates subsequent multi-episodic uplift events during the upper Cretaceous, the Tertiary, and the Quaternary (Freitas, 1951; Melo et al., 1985; Almeida and Carneiro, 1998; Modenesi-Gauttieri et al., 2002; Tello Saens et al., 2003; Hackspacher et al., 2004; Franco-Magalhães et al., 2014), with the uplift of the Serra do Mar mountain range thought to have extended until recent times (i.e., Holocene; Cogné et al., 2012). Despite tectonic processes being active until the Holocene, we assume here that large and more recent landform changes sufficient to isolate populations of birds would be unlikely in SE Brazil. We make this assumption because the uplift rates of these mountains are unknown and a direct test of their role on population divergence timing would be untenable. So, our tested scenario is based on the likely effect of historical climate modulating evolutionary changes onto a long-standing relief.

Available evidence from fossil pollen records in southern and southeastern Brazil highland sampling sites (>900 m a.s.l.) at Mantiqueira, Serra do Mar, and Serra Geral mountain ranges suggests broadly concordant cold and dry conditions during the last glacial maximum, with forests completely absent or restricted to ravines and/or at lower altitudes (Behling, 1997, 2007; Behling and Pillar, 2007; Behling et al., 2007; Oliveira et al., 2008; Ledru et al., 2009; Behling and Safford, 2010; Oliveira et al., 2012). The onset of a moister climate after this period favored the return of montane forest species (Behling, 1997; Behling and Pillar, 2007; Behling et al., 2007; Ledru et al., 2009; Behling and Safford, 2010; Oliveira et al., 2012). Importantly, the highland vegetation seems to have had a complex dynamics during the last 130,000 years BP (i.e., late Pleistocene and Holocene), with multiple shifts in community composition and elevational

distribution of montane forest plant species (Ledru et al., 2009; Behling and Safford, 2010; Oliveira et al., 2012).

SAMPLING AND LABORATORY METHODS

We sampled 90 individuals (50 of *M. cabanisi* and 40 of *M. lateralis*) from nine localities—10 per locality, distributed throughout the species' known distributions (Fig. 1, Table S1). We covered much of the altitudinal range of the organisms, including lowland localities in southern Brazil (∼300 m, Fig. 1, localities 8 and 9) up to more than 1800 m in SE Brazil (Fig. 1, locality 1). Specimens were attracted by playback and collected as described in Amaral et al. (2012) (see Acknowledgments for permits number and Table S1 for specimen and tissue collection holdings).

PALEODISTRIBUTION MODELING

Occurrence records were obtained from the online databases speciesLink (http://splink.cria.org.br/), Global Biodiversity Information Facility http://www.gbif.org; GBIF Occurrence Download DOI 10.15468/dl.8383sp), Ornis (http://www.ornisnet.org/), Xeno-canto (http://www.xeno-canto.org/), Wikiaves (http://www.wikiaves.com.br), and the DVD "Aves do Brasil" (Minns et al., 2010). In addition, label data from study skins were obtained from two Brazilian collections, "Museu de Zoologia da Universidade de São Paulo (State of São Paulo)" and "Museu de História Natural Capão da Imbuia (State of Paraná)". Finally, we also added occurrence records from our own and third-party fieldwork (Fábio Schunck, Fernando Straube, João Marins, Santiago Claramunt). Because *M. cabanisi* was formerly regarded as a subspecies of *M. lateralis*, all occurrence records originally identified as *M. lateralis* south of the São Paulo gap were considered *M. cabanisi* (see Fig. 1). All spatially uncertain records (e.g., discrepant from others or located in the municipality's centroid) were individually evaluated and those whose original source could not be accessed were eliminated. To minimize the effects of sampling bias on model predictions, the occurrences were geographically thinned and only records at least 10 km apart were considered ahead; this procedure was implemented from the "spThin" package in R platform (Aiello-Lammens et al. 2015). A total of 207 cleaned occurrences were recorded for both species (33 for *M. lateralis* and 174 for *M. cabanisi*). Species occurence data, climatic layers, and ENM outputs are available in Dryad (https://doi.org/10.5061/dryad.wh70rxwnn).

We obtained climate layers at 2.5 min resolution from CHELSA (http://chelsa-climate.org/) and PaleoClim databases (http://www.paleoclim.org/) for four key periods across middle/late Pleistocene: present (Karger et al., 2017), Last Glacial Maximum – 21,000 years (Karger et al., 2017), Last Interglacial – 130,000 years (Oto-Bliesner et al., 2006), and the Marine Isotope Stage 19 (MIS19) in the Pleistocene – 787,000 years (Brown et al., 2018). To avoid collinearity, we computed a Principal Component Analysis (PCA) based on the correlation matrix among the 19 bioclimatic variables and selected the five first orthogonal axes as models' predictors, which retained at least 95% of the total variance (De Marco and Nóbrega, 2018). To maintain the dimensionality among the climate predictors through, all the PCA procedure was standardized assuming the current climate as a baseline: (1) first, the bioclimatic variables from all periods were centered and scaled using the mean and standard deviation from the current climate; (2) next, the PCA was first computed using the current climate and then its coefficients were applied to find the axes' scores from the past climates (see standard protocols in Manly et al., 1994 and Legendre and Legendre, 1998). To access the dynamics of species range over time, we interpolated the climate conditions (PCA axes) among these key four periods at 1 ky resolution by using the globally stacked δ^{18} Oxygen curve from Lisiecki and Raymo (2005) as a covariate (see a similar procedure in Lawing and Poly 2011).

Because there is no absolute absence data for modeled species, and to avoid pseudo-models by sampling pseudo-absences (see details in Golicher et al., 2012), we built ecological niche models (ENMs) by using five presence-only methods: Bioclimatic Envelope Score (Bioclim), Ecological Niche Factor Analysis (ENFA), Environmental Distance (Domain or GowerDist), Maximum Entropy (Maxent), and Support Vector Machine (SVM). Using multiple methods is essential to consider uncertainties from ENM predictions (Diniz-Filho et al., 2009). Thus, niche models were calibrated with the current climate and projected onto every 1000 years past climate conditions. All methods were implemented in the R platform by using the functionalities from the "dismo" package (Hijmans et al. 2017), except the SVM, which was implemented from the "kernlab" package (Karatzoglou et al. 2004); Maxent and SVM were implemented with default parameters. The model's performance was evaluated with the D statistic, which considers only presence records and weights the true positive rate (TPR) by the inverse of the proportional predicted distribution area (pi): D = TPR*(1-pi) (Pearson et al., 2007). To compute presence/absence maps, we thresholded the continuous suitability maps based on the 10% of omission error for each ENM for every 1000 years resolution. From binary maps, we computed the area of geographical range for each species, as well as the spatial overlap between them across mountain gaps (see below).

TESTING THE SYNERGY BETWEEN CLIMATE AND TOPOGRAPHY

To test if range dynamics resulted from the interplay between Pleistocene climate changes and topography, we fitted a Generalized Additive Mixed Model (GAMM) to compare the climatic suitability (response variable) of both species in relation to the mean annual temperature and elevation (predictors) across their

geographical ranges over time. Collinearity of predictors was smaller than acceptable thresholds (Pearson's $r = -0.40$, VIF = 1.19; Zuur et al., 2010; Dorman et al. 2013). If both temperature and topography determine species distribution across glacial cycles, then the interaction term of GAMM should be statistically meaningful and the full model including both predictors and the interaction term should be best supported in an AIC framework relative to models including only individual predictors (i.e. temperature or elevation). We also contrasted these models with an intercept-only model (i.e., no predictors); if temperature and elevation do not explain species suitability, the intercept-only model should be favored.

Both response and predictor variables were sampled from three key periods indicating contrasting glacial and interglacial conditions across the last ice age: Holocene (0-6000 years), LGM (18,000-24,000 years), and LIG (120,000-126,000 years). We considered the years delimiting these periods as random effects in GAMM. Because both temperature and elevation are spatially structured along a latitudinal gradient in the study area, we used the latitude to control for spatial autocorrelation. We tested the scenarios by fitting GAMM models considering all predictors (synergy scenario) and each predictor in isolation (temperature or elevation). The smooth terms of all predictors (temperature, elevation, and their interaction) were fitted for each species. All models, including the intercept-only one, were built by considering one intercept for each period (Holocene, LGM, and LIG) and an overall intercept-only.

LABORATORY METHODS

We extracted total DNA from pectoral muscle using the Qiagen DNeasy kit (Valencia, CA) according to the manufacturer's protocol, including an RNAse treatment. We obtained genomic data using sequence capture and Illumina sequencing of ultraconserved elements (UCEs) following standard protocols (Faircloth et al., 2012) after a few modifications: enrichment was done using 650 probes, targeting 634 loci covering all *Gallus gallus* chromosomes; use of 100 bp paired-end Illumina Hiseq 2000 sequencing run, and 16 cycles in both pre- and post-capture PCR reactions. Library preparation was performed by RAPiD Genomics (Gainesville, FL, USA). Raw NGS files and genomic analyses are available in Dryad (https://doi.org/10.5061/dryad.wh70rxwnn).

SEQUENCE QUALITY CONTROL, MTDNA, UCE ASSEMBLY, AND SNP CALLING

We sorted raw sequences by individual tags using Illumina's Casava software. Initial quality control was performed using FastQC 0.10.1 (Andrews, 2014). Adapters, barcodes, and low-quality regions were trimmed using Illumiprocessor 2.0.7 (Faircloth, 2014), which processes Illumina sequences using Trimmomatic 0.32.1 (Bolger et al., 2014). Assembly, removal of non-UCE loci, and final loci alignment were performed with Phyluce 1.4 (Faircloth 2014). The largest contig of each locus was used as a reference for mapping individual reads using BWA-mem (Li 2013). We used Picard (Broad Institute, Cambridge, MA; http://broadinstitute.github.io/picard/) to perform filtering steps on Bam files. We trimmed read ends with CleanSam.jar, reassigned reads to groups with AddOrReplaceReadGroups.jar, and excluded duplicated reads with MarkDuplicates.jar. The Bam files for all individuals were combined and SNPs were called using GATK version 3.6 (McKenna et al., 2010). We kept only >Q30 SNPs for downstream analyses. We sampled one random SNP per locus from the collection of all zero-missing biallelic SNPs recovered for the locus. We removed Z-linked SNPs using a local BLAST search based on the zebra-finch Z chromosome (Emsembl taeGut3.2.4) to avoid any bias due to the idiosyncratic evolution of sex chromosomes and different ploidy (the number of recovered Z-linked SNPs was limited and thus, they were not used in any analysis). We obtained phased sequences for UCEs loci using seqcap_pop (Harvey et al. 2016).

Since mtDNA is a common subproduct of sequence capture experiments (see Amaral et al., 2015), we also isolated complete cytochrome b sequences from assemblies that were generated by Phyluce using a local BLAST search based on the complete mitogenome of *Microspingus lateralis* (Genbank NC_028039.1) to obtain a Median Joining Network using POPART version 1.7 (Leigh and Bryant, 2015). Mitochondrial sequences are available under Genbank numbers MZ417229-MZ417313.

POPULATION STRUCTURE

We explored population structure with sparse non-negative matrix factorization (sNMF, Frichot et al., 2014, implemented in the R package LEA, Frichot and Olivier, 2015) and with a multivariate Discriminant Analysis of Principal Components (Jombart et al., 2010). The sNMF runs were performed for a range of K values from 1 to 9 (following the number of sampling localities), with 500 runs per K. We used the minimum cross-entropy method to identify the best fitting K. Runs with the lowest values of minimum entropy were selected. Since sNMF's regularization parameter alpha may affect the inferences (Frichot et al., 2014), we evaluated the results under different values of alpha (1, 10, 100, and 1000). To further assess population structure we ran a DAPC analysis using a k-clustering algorithm to determine the *a priori* grouping of individuals based on the Bayesian Information Criterion (BIC). The first set of principal components accounting for 80% of the variance was included in the analyses.

INFERENCE OF HISTORICAL PROCESSES

Based on the results from the previous analyses that recovered three populations (Fig. 2), we tested a suite of alternative models to assess the most likely differentiation scenario for

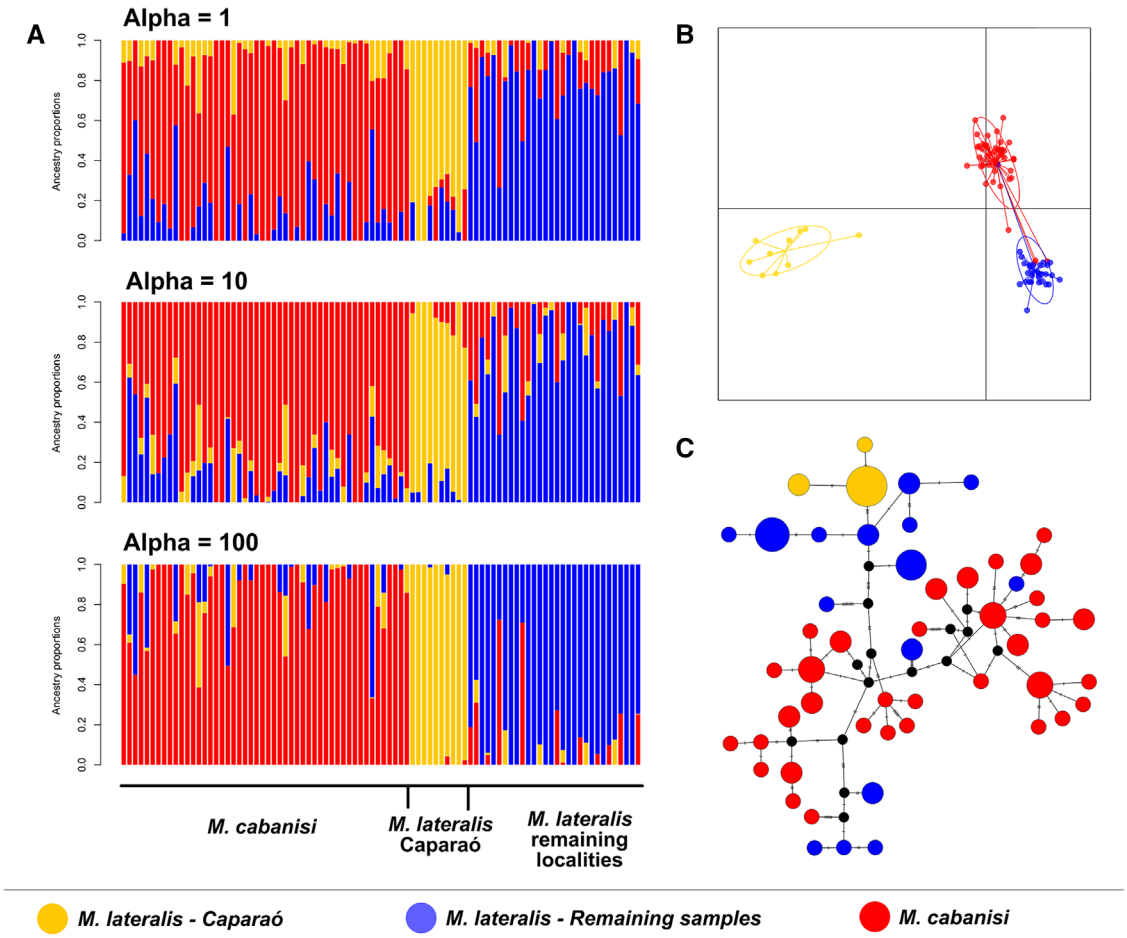

Figure 2. Plots depicting population structure according to (A) the best fitting sNMF model K = 3 based on different values of the regularization parameter alpha (1, 10, 100), (B) the three clusters inferred with DAPC, and (C) cytochrome-b median-joining network. Black dots in the haplotype network indicate inferred haplotypes.

Microspingus lineages. The models tested explored the relationships of the three genetic clusters inferred by sNMF and DAPC, the presence of gene flow, and instantaneous population size change after divergence (Fig. 3). Given a large number of possible discrete demographic histories among the three inferred populations, we performed model selection using hierarchical approach using a neural network algorithm (see below), by first contrasting the support for alternative topologies followed by a comparison among distinct demographic scenarios. For the topology test, we explored six models including three alternative topologies and the presence of gene flow between the Caparaó population and the remaining individuals of *M. lateralis* (Fig. 3). The modeled topologies were as follows: m1_23 and m1_23_B - (*M. cabanisi*,(*M. lateralis*, Caparaó)); m3_12 and m3_12_B - (Caparaó,(*M. lateralis, M. cabanisi*)); m123 and m123_B - the simultaneous divergence between the three taxa (*M. cabanisi, M. lateralis*, Caparaó). We did not consider models assuming *M. cabanisi* and the Caparaó population as sisters given that southern *M. lateralis* is sandwiched by these two geographically distant populations (Fig. 1). Thus, a shared ancestry is less likely, and furthermore confirmed by our cluster analyses (see results; Fig. 2B). For each topology, we tested models with and without (_B models) gene flow between populations. For estimating parameters under the best fit historical demographic model, we simulated a new set of scenarios under the best model resulting from the topology test. Specifically, we estimated parameters describing population size changes (Figure 3B). Here, demographic models had additional parameters that were related to both the time and magnitude of population size changes We assumed that the effective size of ancestral populations (before instantaneous population size changes), could have been larger (contraction) or smaller (expansion) than the current populations. Models differ from each other by which populations were allowed to change in size through time (Fig. 3B).

To simulate genetic data under the described demographic models we used the package PipeMaster (Gehara et al. 2017), which employ the msABC coalescent-simulator (Hudson, 2002; Pavlidis et al., 2010) to generate genetic data and the PopGenome

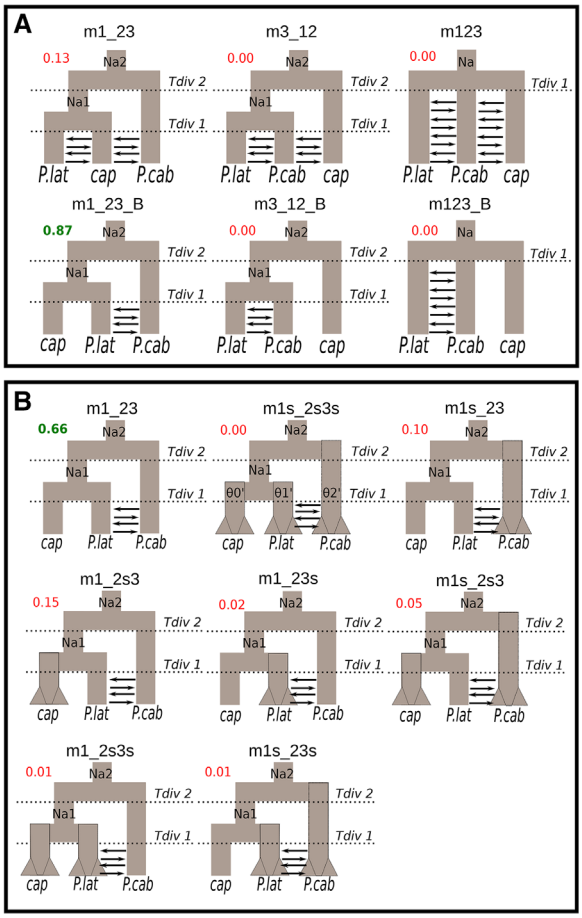

Figure 3. Demographic models tested with our supervised machine learning approach using a nonlinear neural network algorithm. We tested distinct models using a hierarchical approach. Initially, we tested models varying topology between *Microspingus cabanisi*, *Microspingus lateralis*, and Caparaó population, and the presence of gene flow among the *M. lateralis* and Caparaó population (the most isolated population; A). After the topology test, we simulated a new set of scenarios under the best model testing different variations of population size changes (B; demography test). For testing population size changes, we allowed different sets of populations to expand or contract in size after the divergence. Numbers with colors (red and green) are probabilities for model selection using 75% of the simulations as training data and the remaining 25% as testing. In green are the models with the highest probabilities.

(Pfeifer et al. 2014), for summary statistics calculation. PipeMaster randomly selects parameter values for each simulation from uniform prior distributions which are informed by the user. We specified broad and poorly informative prior to all the parameters (Table 1). By using Pipemaster we were able to: (1) account for the uncertainty on the mutation rate, assuming a prior distribution where distinct values are drawn for each locus, (2) perform a power analysis to explicitly test how well models can be differentiated given the observed data, and (3) estimate demographic parameters without the need to inform the proportion of monomorphic sites. We conducted 100,000 simulations per model and calculated the following summary statistics: number of segregating sites (S) per taxa and for all individuals combined, nucleotide diversity (π) per taxa and for all individuals combined, Watterson's theta (θ; Watterson, 1975), Tajima's D (Tajima, 1989), pairwise F_{ST} (Wright, 1949), Fay and Wu's H (Fay and Wu, 2000), the proportion of shared alleles between taxa, the proportion of private alleles in each taxon, and the proportion of fixed alleles in each taxon. Similarly, we used PipeMaster to calculate the same summary statistics for the observed data. Given that simulated summary statistics were conducted under known parameter values (sampled from uniform distributions), we used this data set to train a machine-learning algorithm to infer model probabilities and parameter estimates from observed summary statistics. To check if simulated data could generate summary statistics similar to the observed data, we conducted a PCA and visually inspected if the observed data was within the simulated data cloud on the first four principal components. To perform model classification we used a nonlinear neural network (nnet) algorithm on the R package caret version 6.0-84 (Kuhn et al., 2019). To estimate which combination of the number of internal nodes and decay values produces the maximum accuracy, we performed 20 bootstraps replicates with 2,000 iterations in each learning replicate. We used 75% of the simulations as training data and the remaining 25% as testing. We summarized model classification accuracy plotting heatmaps of the confusion matrices (Figure 8). To estimate the parameters for the best model we simulated additional data, producing a total of 1,000,000 simulations, and used the neuralnet algorithm from the functions abc of the ABC version 2.1 package (Csilléry et al., 2012). The abc function initially conducts a rejection step using a specific tolerance level, selecting a proportion of the simulations closer to the observed data set prior to executing the neural network approach. To evaluate which tolerance level produces the higher accuracy in parameter estimation we used the function cv4abc of the ABCpackage with 100 replicates. We explored three different tolerance levels 0.05, 0.01, and 0.001 retaining 50,000, 10,000, and 1000 simulations, respectively. We evaluated the best tolerance level by estimating the predicted error of parameters, selecting the tolerance level with the lowest error rate to perform parameter estimation. Additionally, we estimated Pearson's correlation index between simulated and pseudo-observed data sets for the best tolerance level to access parameter estimation accuracy.

Table 1. Parameters estimated under the best demographic model m1_23 (Fig. 3) - (*M. cabanisi*, (*M. lateralis*, Caparaó)) without population size changes], assuming a tolerance level of 0.001 (1000 simulations). Ne - effective population size; Tdiv 1 - the divergence time in years between *Microspingus lateralis* and Caparaó; Tdiv 2 - the divergence time in years between *M. cabanisi* and *M. lateralis*+Caparaó; mig cab → lat - migrants per generation from *M. cabanisi* to *M. lateralis*; mig lat → cab - migrants per generation from *M. lateralis* to *M. cabanisi*; μ - mutation rate.

	Ne *M. cabanisi*	Ne *M. lateralis*	Ne Caparaó	Tdiv 1	Tdiv 2	mig cab → lat	mig lat → cab	μ
Prior	50k-2000k	50k-2000k	1k-150k	1k-500k	1k-500k	0.1-4.0	0.1-4.0	1E-11 – 5E-9
2.5 % Perc.:	1,491,022	1,084,595	85,823	28,032	65,318	2.98	2.82	9.15E-10
Median:	1,597,792	1,157,056	95,135	40,701	81,234	3.09	2.90	9.94E-10
Mean:	1,594,627	1,158,880	94,454	40,892	81,096	3.10	2.89	9.89E-10
Mode:	1,610,541	1,148,219	96,856	42,111	83,380	3.09	2.90	1.00E-09
97.5 % Perc.:	1,680,424	1,235,116	99,343	55,593	97,708	3.21	2.97	1.05E-09

Table 2. Scenario tested, model performance and model selection among Generalized Additive Mixed Models - GAMMs.

Scenario	Predictor	R^2	AIC	delta_AIC
Synergy	Period+s(Temp)+s(Elev)+ti(Temp, Elev)	0.73	22014	0
Temperature	Period+s(Temp.)	0.63	27848	5833
	s(Temp.)	0.60	292881	270867
Precipitation	Period+s(Elev.)	0.63	29725	7710
	s(Elev.)	0.61	29305	7291
-	Intercept-only (by Period)	0.11	46659	24644
	Intercept-only (overall)	–	3344948	3322934

Results

PALEODISTRIBUTION MODELING

Niche models satisfactorily predicted the northern and southern geographic distributions of *M. lateralis* and *M. cabanisi*, respectively (Fig. 4). Both species showed cyclic paleodistribution dynamics over the last 800,000 years, with range expansion during cooler glacials and contraction during warmer interglacials (Fig. 4 and Animation S1). During warmer periods when distributions were narrower, niche models predicted two gaps isolating the two species from each other and the Caparaó population from the remaining populations within *M. lateralis* (Fig. 5). Throughout this cyclic paleodistribution dynamics, the geographic range of *M. lateralis* remained discontinuous along the northern gap for a longer period of time relative to the isolation between *M. lateralis* and *M. cabanisi* along the southern gap (Figure 5).

In general, both species tolerate similar mild temperatures (10-22°C), but occupy regions with distinct elevations (Figure 6). The northern species, *M. lateralis*, compensates the hotter climates at lower latitudes by occupying only higher elevations compared to its southern relative *M. cabanisi* (Figure 7). Not surprisingly, GAMM results indicate a significant interaction between temperature and elevation in explaining the climatic suitability of both species (Table S2), with the full model including the additive effect of these predictors and their interaction selected by AIC framework (Table 2); that is, the temperature of an occupied pixel is not independent of its elevation. In other words, GAMM corroborated the synergy between climate and topography in determining species range across time and geography.

SEQUENCING RESULTS

We obtained 8465 SNPs that passed our quality filtering from a total of 634 UCE loci (median length: 633 bp, range: 216–811 bp). Each UCE locus had a median of 13 SNPs (range: 1–35). The final dataset containing one randomly sampled SNP per variable autosomal locus had 588 SNPs. Cytochrome b data was obtained for 85 of the 90 samples, excluding four *M. lateralis* (FRA03, MV01, FRA07, and FRA09) and one *M. cabanisi* (FRA29).

POPULATION STRUCTURE

Our sNMF runs indicated three groups based on the best cross-entropy across alpha values, except for alpha of 1000, which showed a smaller cross-entropy value for a single group (Figure S1). Plots based on alpha of 1, 10, and 100 for $K = 3$ support the Caparaó population of *M. lateralis*, the remaining *M. lateralis* populations, and *M. cabanisi* as three distinct clusters with somewhat varying levels of mixed ancestry coefficients (Fig. 2), while a plot based on alpha of 1000 supports $K = 1$. DAPC based on k-clustering algorithm suggests two as the best

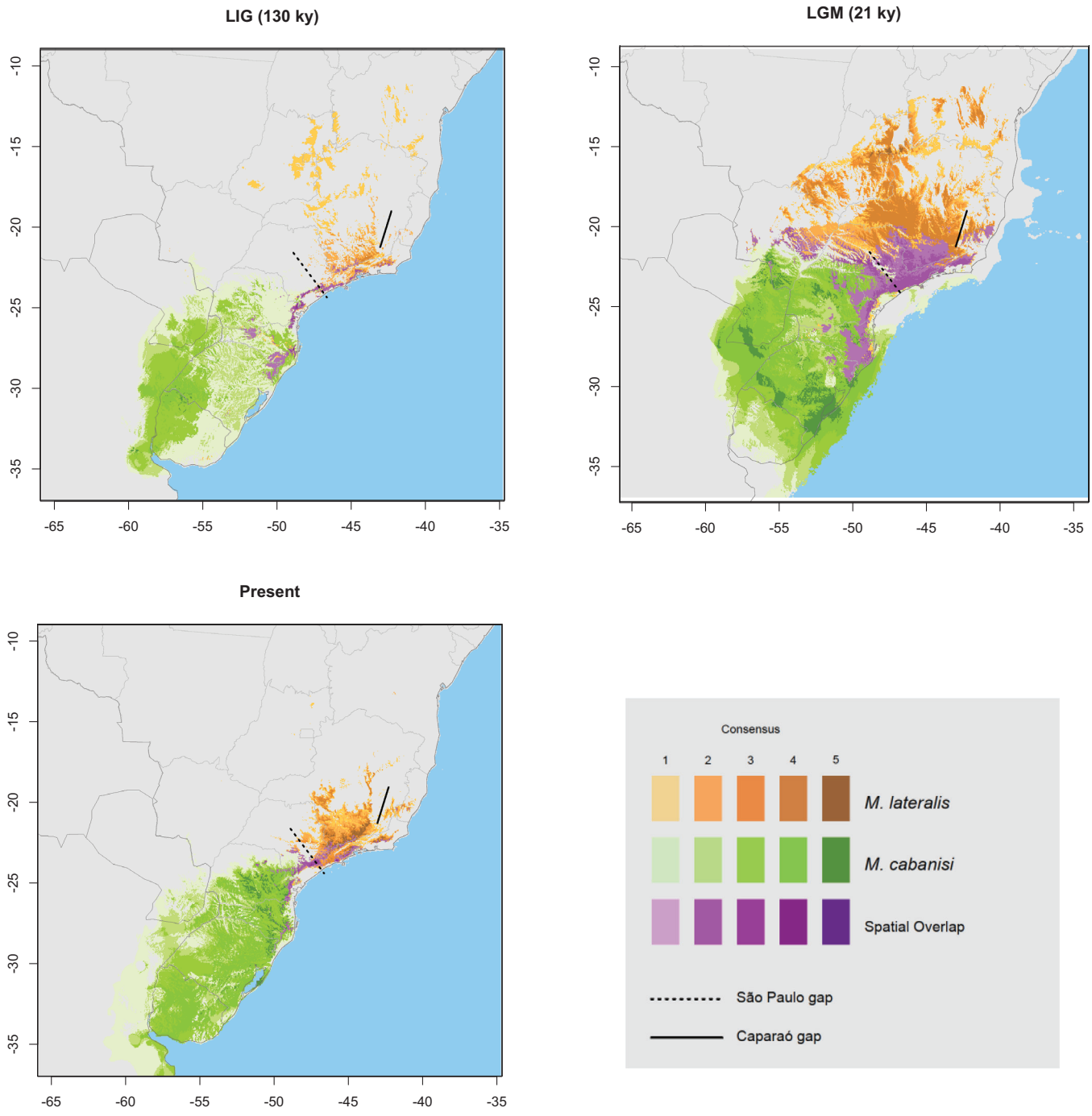

Figure 4. Geographic distribution of *M. lateralis, M. cabanisi* and their spatial overlap during the last interglacial (126,000 years), last glacial (21,000 years) and present. The consensus indicates the number of models predicting species presence across space.

number of groups, although BIC values are very similar among K = 1, K = 2, and K = 3 (246.7343, 246.5362, and 247.0419, respectively; Figure S2). These two clusters correspond to: (1) the Caparaó population of *M. lateralis* + some *M. cabanisi* individuals and (2) remaining *M. lateralis* individuals + remaining *M. cabanisi* individuals (Fig. S2). If the three sNMF populations are considered in the DAPC analysis instead of the groups defined by the k-clustering algorithm, the groupings are similar: one of them included only *M. lateralis* Caparaó individuals and the other two reunited mostly individuals of either *M. cabanisi* or *M. lateralis* (Fig. 2). Accordingly, the mtDNA haplotype network did not show shared haplotypes either between the two species or between the Caparaó population and the other individuals. However, some haplotypes of *M. lateralis* were more closely related

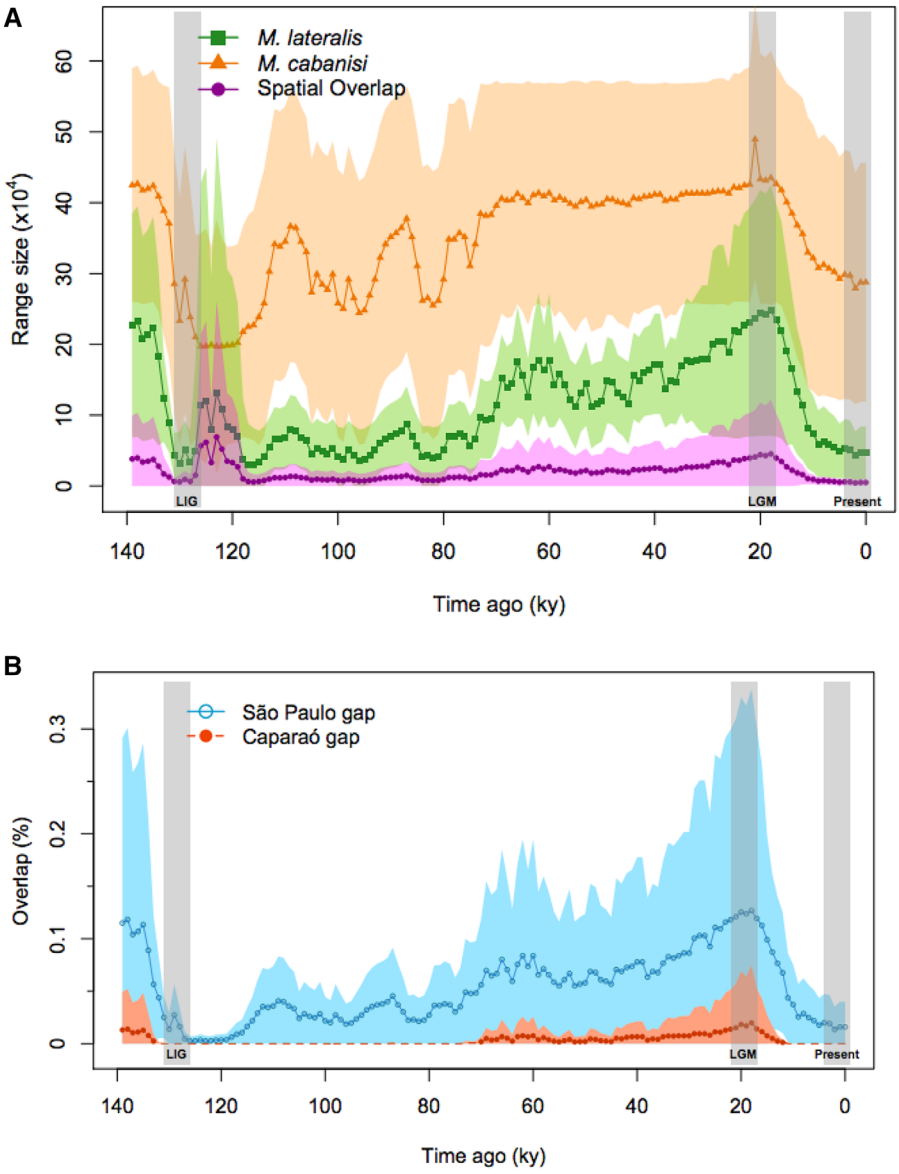

Figure 5. Magnitude of geographical range size (A) of *M. lateralis* and *M. cabanisi* and their spatial overlap (B) through time.

to those of *M. cabanisi* than to conspecific ones (Fig. 2). We used K = 3 in downstream analyses despite potential gene flow between *M. cabanisi* and *M. lateralis* as this number of populations is congruent with plumage variation (Assis et al., 2007), geography, and population structure.

DEMOGRAPHIC RELATIONSHIPS AND POPULATION HISTORY

For the topology test, our machine learning approach identified the correct model in 85% of the simulations, suggesting high confidence in model selection (Fig. 8). The best model among alternative topologies and distinct scenarios of gene flow supported an initial differentiation between *M. cabanisi* and *M. lateralis*, followed by the split between the Caparaó population and the remaining individuals of *M. lateralis*, without subsequent gene flow between the latter (m1_23_B, probability = 0.87; accuracy = 0.776; Table 2; Fig. 4). The PCAs indicated a good fit of simulated models to the data, with the observed data clustering with the simulations in the first four PCs (Fig. S3). For the demography test, our approach suggested relatively low confidence in model selection (average accuracy = 0.40). The models with the highest accuracy had no effective population size changes (m1_23, accuracy = 0.65) or population size changes in all three populations (m1s_2s3s, accuracy = 0.84; Fig. 3). Here, the best-supported model suggested stable population sizes for all three populations (m1_23; probability = 0.66; Table 2, Figure 3).

The cross-validations for parameter estimation produced the lowest error rates under a tolerance level of 0.001 (1,000

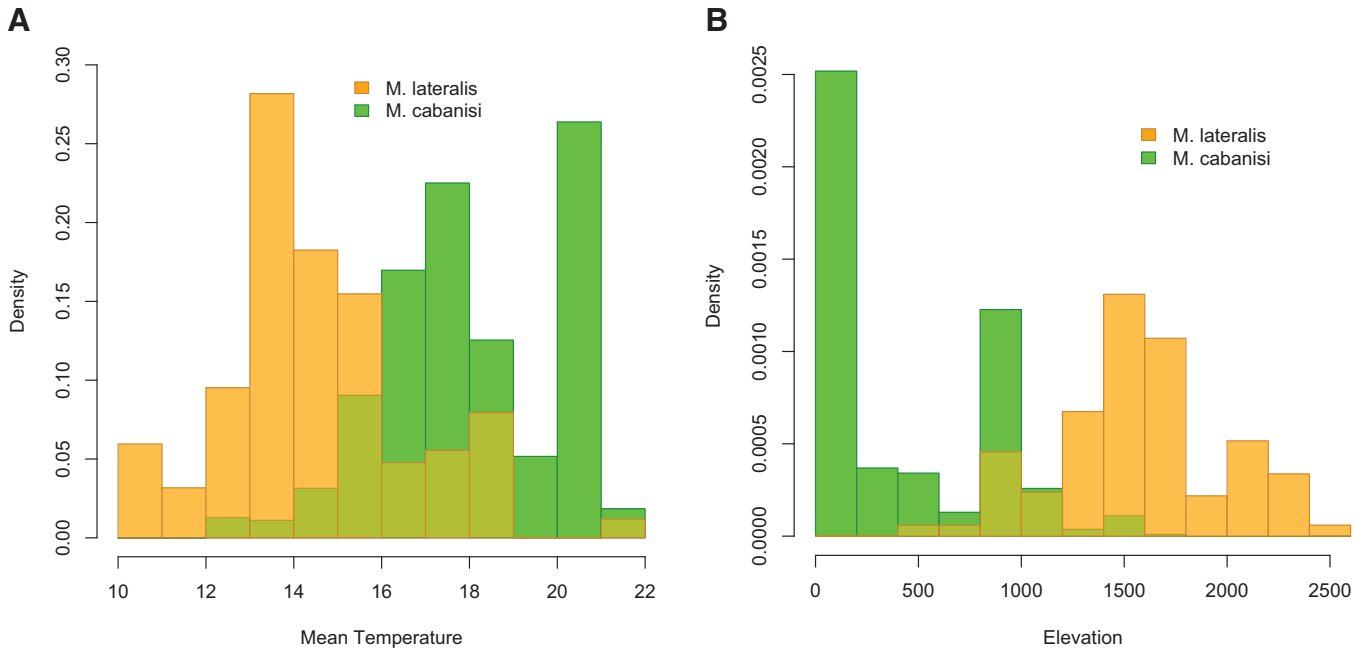

Figure 6. Frequency of mean annual temperature (A) and elevation (B) across the geographical range of *M. lateralis* and *M. cabanisi*.

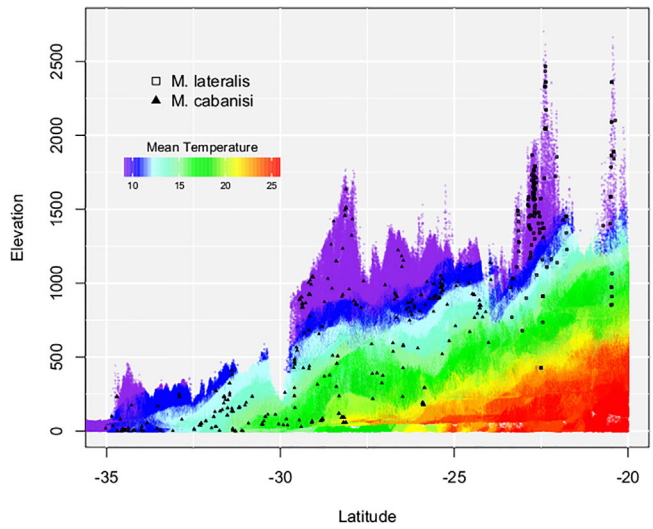

Figure 7. Occurrence of *M. lateralis* and *M. cabanisi* across the latitudinal, altitudinal, and thermal gradients.

simulations; average error rate = 0.17; Table S3). The lowest values for Pearson's correlation index between simulated and pseudo-observed data were estimated for migration parameters (average r^2 = 0.80) and mutation rate (r^2 = 0.72; Table S4). Parameter estimation for our best model [m1_23 - (*M. cabanisi*, (*M. lateralis*, Caparaó)) without population size changes] supported current effective population sizes concordant with the currently occupied area by the three populations, with *M. cabanisi* having the largest population size (mean = 1,594,627, 95% CI = 1,491,022 - 1,680,424) and the largest distribution, and Caparaó population having the smallest effective population size (mean = 94,454, 95% CI = 85,823 - 99,343) and the smallest range. Divergence among populations occurred relatively recently, with the initial split between *M. cabanisi* and *M. lateralis* g at 81,096 years ago (mean; 95% CI = 65,318-97,708), followed by the split between *M. lateralis* and the Caparaó population at 40,892 years ago (mean; 95% CI = 28,032-55,593). Gene flow was relatively high and took place after the divergence between *M. cabanisi* and *M. lateralis*, with an average of 2.95 migrants per generation (Table 1).

Discussion

INTERPLAY BETWEEN CLIMATE AND TOPOGRAPHY

Our findings indicate that an interaction between climate and topography likely shaped the diversification of the two tropical cold-associated sister warbling finches, based on both demographic and distribution modeling. This is supported by the AIC approach and the GAMM models (Fig. 3, Tables 1 and 2), which showed that the historical interplay between temperature and elevation significantly explain the climatic suitability of both species. Additionally, the paleodistribution models (Fig. 4–5) seem to be in line with the demographic modeling results, indicating that the colder climate of the last glacial period enabled higher connectivity of formerly isolated and already diverged populations, which possibly led to the historical hybridization between the two species. However, our demographic modeling places the events that originated the three modern genetic

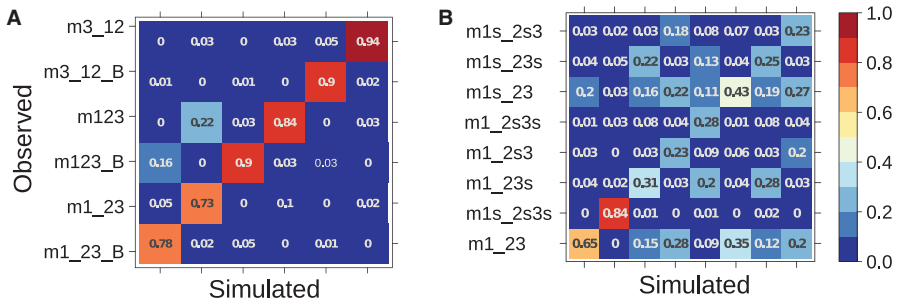

Figure 8. **Confusion matrix for the two sets of simulated demographic models (A, Topology test; B, demography test), obtained with a nonlinear neural network algorithm. Model names are the same as in Figure 3. Numbers in the cells represent the proportion of the testing data that was assigned to each of the simulated models. Values in the diagonal represent the models' classification accuracy.**

clusters to the early stages of the last glacial period, which does not support the expectations of the interaction between climate and topography. In the following, we discuss our results in light of this scenario.

One potential cause for the discrepancy between the divergence time estimates (Table 1) and the expectations from the synergy between climate and topography can be a consequence of the atypical higher amplitude of warmer and colder climates of the last glacial period, its long duration (ca. 100,000 years) and a slow pace of cooling to full glacial conditions (Flantua and Hooghiemstra, 2018). This could have generated a time lag in the completion of upslope isolation that was triggered during the previous interglacial. In fact, confidence intervals of divergence estimates indicate that all lineage separation took place before the last glacial maximum (i.e., more than 21,000 years ago), when cold-associated organisms were presumably more widely connected. Further support to this scenario is given by paleodistribution modeling results, which showed that during the last interglacial, the ancestor of the two species was already isolated across the southern gap (Figure S2b). This low connectivity lasted until the early glacial period (ca. 80,000-70,000 years), coinciding with the divergence time estimated from the demographic modeling. Moreover, the paleodistribution models indicated that the amount of range overlap and connectivity between the two species varied during the last glacial period. This underscores a scenario in which cooling did not follow a linear pattern after the last interglacial and that evolutionary dynamics of cold-associated neotropical organisms might not fit a purely dichotomous glacial and interglacial scenario of diversification.

Alternatively, montane habitats and cold-associated organisms could have been isolated in high or mid-elevations due to the effects of increased aridity independent of cooling during the last glacial. Indeed, palynological studies in the highlands of eastern Brazil pointed to paired cold and dry conditions during the LGM (Behling, 1997, 2007; Behling and Pillar, 2007; Behling et al., 2007; Oliveira et al., 2008; Ledru et al., 2009; Behling and Safford, 2010; Oliveira et al., 2012). Thus, an increasingly dry climate since the onset of the last glacial period would have promoted isolation and differentiation in distinct montane refugia. However, such a scenario would predict the highest likelihood of montane habitat fragmentation and isolation during the LGM in MAF (i.e., a dry montane refugia; Ramírez-Barahona and Eguiarte, 2013). This is at odds with our paleodistribution modeling results that suggest high biogeographical connectivity, rather than isolation, during this period, and with our divergence time estimates, which indicate population differentiation predating the LGM. Finally, the difficulties brought by the limited knowledge on substitution rates of UCEs and generation times of Neotropical birds adds an additional layer of uncertainty in divergence time estimation that should be further explored in future studies.

Our results also suggest that the interplay between climate and topography, and its effects on population connectivity and isolation varies at the regional scale; that is, it was seemingly idiosyncratic regarding latitude (i.e., the inter-mountain gaps are in distinct sectors) and topographic complexity (i.e., the two gaps are situated in Serra do Mar and Mantiqueira ranges, Fig. 1). For example, the divergence time between the two species (ca. 80,000 years) and between the Caparaó and remaining populations within *M. lateralis* (ca. 40,000 years) occurred on distinct and non-overlapping time periods. Specifically, both demographic and paleodistribution modeling indicate that while populations became isolated and diverged across the northern gap at about 55,000-30,000 years, a concomitant increasing pattern of connectivity between the two species took place across the southern gap. These findings support the mountain flickering connectivity model in tropical mountains, whereby patterns of connectivity and fragmentation can occur at distinct temporal scales within and across mountain regions (Flantua and Hooghiemstra, 2018; Flantua et al., 2019).

GENOMIC INTEGRITY AND INTROGRESSION

Zones of putative secondary contact and hybridization between previously isolated highland populations have been observed in

other tropical (Kadereit 2015; Diazgranados and Barber, 2017; Winger, 2017) and temperate (Hewitt 1996, 1999, Galbreath et al., 2010) regions. Our paleodistribution modeling analyses suggest that range overlap between the two species started at about 80,000-70,000 years and peaked at ca. 30,000-15,000 years across the southern gap (Fig. 5) and are consistent with the demographic modeling results of introgressive hybridization following divergence. The role of past introgression in shaping modern patterns of genetic diversity is further supported by shared polymorphisms and genetic similarity of southern *M. lateralis* with respect to *M. cabanisi* (Fig. 2A, B). In fact, assuming that gene flow is not overestimated in our study system, it is intriguing that despite historical range overlap and a rate of gene flow high enough to render genomic homogenization (i.e. 2.95 individuals/generation; Slatkin, 1985), the integrity of the two divergent genomes/phenotypes was apparently protected until these forms were reduced to their current allopatric ranges. This implies that some kind of postzygotic barriers could have hindered the fusion of the two genomes when populations resumed secondary contact (Barton, 1983; Barton and Hewitt, 1985; Barton and Gale, 1993), or that the nature of the population histories and gene flow are underpinned by complex spatial dynamics that deviate from our simplified model that involves multiple panmictic population connected by shared ancestry and continuous gene flow rather than episodic pulses. Signs of introgression between *M. cabanisi* and the southern population of *M. lateralis* may pave the way to future studies testing more detailed hypotheses, including a possible hybrid origin of *M. lateralis*, with an experimental design specific to that end (i.e., a much larger SNP dataset).

POPULATION STRUCTURE RELATIVE TO OTHER NEOTROPICAL MONTANE, COLD-ASSOCIATED AND MAF SPECIES

The strong population structure found here (Fig. 2B) is consistent with the observed patterns in other Neotropical montane systems (e.g., Andes), where diversification was likely a consequence of allopatric isolation in response to complex topography and cyclic climatic changes (Perez-Eman, 2005; Gutiérrez-Pinto et al., 2012; Valderrama et al., 2014; Winger and Bates, 2015; Cadena et al., 2019). However, the lineages recovered in our study and their recent origin contradict previous studies on other organisms ranging broadly in MAF, the latter which did not recover obvious phylogeographic breaks (e.g., Batalha-Filho et al., 2012; Peres et al., 2015) or recovered much older splits (e.g., Pulido-Santacruz et al., 2016, Pie et al., 2018; Peres et al., 2018; 2019). These findings suggest that although warbling finches are forest-associated species that often use forest edges (Jaramillo, 2020a, 2020b), such ecological flexibility was presumably not sufficient to preclude isolation and divergence. In contrast, a sympatric and ecologically similar bird, the White-browed Warbler (*Myiothlypis leucoblephara*), for example, did not show detectable population structure (Batalha-Filho et al., 2012) - as in other more distantly related, co-distributed MAF organisms (e.g., spiders, Peres et al., 2015). Such lack of congruence may be due to the interaction of ecological traits (e.g., related to physiology or ecology) with historical processes (see Zamudio et al., 2016 for a review), differences in altitudinal distribution, lack of power of datasets with a limited number of loci to detect shallow divergences (see Amaral et al., 2018) or a combination of all these factors. This warrants additional studies on both novel and previously studied organisms using subgenomic or whole genome datasets.

ELEVATIONAL DISTRIBUTION AND DIVERGENCE

Variations in altitudinal ranges across a latitudinal gradient can be relevant to the process of geographic differentiation and speciation. The elevational distributions of the two *Microspingus* warbling finches differ, with populations of northern *M. lateralis* being found only above 900 m, while the southern *M. cabanisi* reaches sea-level in the southernmost part of its range. Interestingly, the former has a marked genetic subdivision associated with barriers, whereas no geographic structure was recovered in the latter (Fig. 2A,B). Differences in altitudinal ranges between the two species may be a consequence of thermal niche divergence (Janzen, 1967), biological interactions (i.e., competition), or simply a latitudinal compensation of elevational distribution (Barry, 1992). The remarkable degree of genetic structure attained by the northern populations could be due to (i) a stronger interaction between topography and climate, (ii) a larger propensity of the more linear ranges of cold-associated organisms in this sector of MAF to become fragmented (Graves, 1988), or (iii) populations being less adapted to wider temperature variation (Janzen, 1967; Thom et. al. in prep). Distinct levels of endemism in different portions of MAF could be explained by this hypothesis, underscoring the importance of additional studies of AF co-distributed taxa.

Conclusions

Our study brings valuable insights into the evolution of tropical montane and cold-associated organisms. First, it unfolds a complex role of cyclical climatic changes in association with a long-standing rugged landscape on diversification dynamics. On one hand, as predicted by biogeographic models, our analyses indicate that populations diverged in higher elevations, followed by secondary contact and introgression at lower elevations. On the other hand, the origin of modern genetically divergent populations estimated to early stages of the last glacial period challenges the well-established notion that upslope isolation and divergence of montane organisms took place exclusively during the interglacial periods. One implication here is that range

shifts might lag when responding to historical climate changes. Second, population divergence and connectivity were asynchronous between mountain chains, suggesting that regional idiosyncrasies may play an important role when explaining global patterns of diversification in tropical montane organisms. Third, the spatio-temporal approach implemented here, combining climatic suitability models with additive regression models, can provide a platform for future studies to test the influence of historical elevational range shifts as drivers of diversification in a wide array of montane organisms.

AUTHOR CONTRIBUTIONS

F.R.A. conceived the study. F.R.A., M.M.C., G.T., M.S.L.R., and D.F.A.S. designed the study and analyses. F.R.A., J.A.C.M., and G.T. performed fieldwork. F.R.A., G.T., and D.F.A.S. performed genetic data analysis. M.S.L.R. performed niche modeling analyses. F.R.A., K.C.M.P., C.Y.M., and M.J.H. contributed funds for lab or fieldwork. F.R.A., M.M.C., M.S.L.R., and G.T. wrote the manuscript with input from other authors. All authors approved the final version of the manuscript.

ACKNOWLEDGMENTS

We thank C. Assis, A. Bianco, B. Genevcius, G. Macedo, D. N. Oliveira, V. Q. Piacentini, R. Quagliano, C. F. Schwertner, and J. Vitto for their excellent field assistance. Fábio Schunck, Fernando Straube, João Marins, Santiago Claramunt provided sample localities for niche modeling. Special thanks to B. Faircloth for providing extensive help with UCE processing and SNP calling. ICMBio provided collection permits (14673, 30829, 30835, 30836, 30837, 30838, 30840, 30841, 30844, 37011, 39935, and 47205) and access to National Parks (P. N. Caparaó., P. N. Serra da Bocaina, P. N. São Joaquim, P. N. Serra Geral, P. N. Aparados da Serra). This research has been evaluated by UNIFESP Ethics Committee (CEP 0069/12). D. N. Oliveira helped with lab work. We also thank private landowners for access to land under their care. Financial support was provided by FAPESP and the BIOTA program (2011/50143-7, 2011/23155-4, 2015/18287-0, 2014/00113-2, 2015/12551-7, 2016/11439-1, 2017/25720-7, 2018/17869-3), two joint NSF, FAPESP and NASA grant (Dimensions US-Biota-SP, FAPESP 2013/50297-0/NSF DOB 1343578 and FAPESP 18/03428-5/DEB 1831560), CNPq (312697/2018-0, 306204/2019-3) and Coordenação de Aperfeiçoamento de Pessoal de Nível Superior - Brasil (CAPES) - Finance Code 001. This paper is a contribution of the National Institutes for Science and Technology (INCT) in Ecology, Evolution and Biodiversity Conservation, supported by MCTIC/CNPq (proc. 465610/2014-5) and FAPEG (proc. 201810267000023). For helpful discussions we thank Scott V. Edwards, J. M. B. Alexandrino, M. Pie, A. C. Carnaval, C. Assis, Fernando D'Horta, V. Q. Piacentini, Cibele Biondo, Gabriel Macedo. Camila Marques, Guilherme Cavicchioli, Marcel Neves, Deborah Nacer, Flavia Mobili, Samantha Palhano, Bruna Gimenez, Estela Silva and the FAPESP/NSF AF-Biota group. Finally, we thank Associate Editor Joseph Tobias and two anonymous reviewers for excellent comments on previous versions of this manuscript.

DATA ARCHIVING

Both raw and processed files are available in the public repositories, and were mentioned in the current version of the manuscript (raw sequence data: SRA PRJNA727622; mtDNA sequences: Genbank MZ417229-MZ417313, and genomic and niche analyses files: Dryad https://doi.org/10.5061/dryad.wh70rxwnn).

CONFLICT OF INTEREST

The authors declare no conflict of interest.

REFERENCES

Aiello-Lammens, M. E., R. A. Boria, A. Radosavljevic, B. Vilela, and R. P. Anderson. 2015. spThin: an R package for spatial thinning of species occurrence records for use in ecological niche models. Ecography. 38:541–545.

Almeida F. F. M., and C. D. R. Carneiro. 1998. Origem e evolução da Serra do Mar. Rev. Brasil. Geoc. 28:135–150.

Amaral, F. R., Piacentini, V. Q., Brito, G. R. R., and F. F. Curcio. 2012. A simple and effective air shotgun for collecting small birds and other vertebrates at close range. J. F. Ornithol. 83:403–406.

Amaral, F. R., Neves, L. G., Resende, M. F. R., Mobili, F., Miyaki, C. Y., Pellegrino, K. C. M., and C. Biondo. 2015. Ultraconserved elements sequencing as a low-cost source of complete mitochondrial genomes and microsatellite markers in non-model amniotes. PLoS One 10.

Amaral, F. R., Maldonado-Coelho, M., Aleixo, A., Luna, L. W., Rêgo, P. S. do, Araripe, J., Souza, T. O., Silva, W. A. G., and G. Thom. 2018. Recent chapters of Neotropical history overlooked in phylogeography: Shallow divergence explains phenotype and genotype uncoupling in *Antilophia* manakins. Mol. Ecol. 27:4108–4120.

Andrews, S. 2014. FastQC: A quality control tool for high throughput sequence data. https://www.bioinformatics.babraham.ac.uk/projects/fastqc/

Antonelli, A. 2015. Biodiversity: Multiple origins of mountain life. Nature 524:300–301.

Antonelli, A., Kissling, W. A., Flantua, S. G. A., Bermúdez, M. A., Mulch, A., Muellner-Riehl, A. N., Kreft, H., Linder, H. P., Badgley, C., Fjeldså, J., et al. 2018. Geological and climatic influences on mountain biodiversity. Nature Geoscience 11:718–725.

Assis, C. P., Raposo, M. A., and R. Parrini. 2007. Validação de *Poospiza cabanisi* Bonaparte, 1850 (Passeriformes: Emberizidae). Rev. Bras. Ornitol. 15:103–112.

Barry, R. G. 1992. Mountain weather and climate, Third edit. ed. Cambridge University Press.

Barton, N. H. 1983. Multilocus clines. Evolution 37:454–471.

Barton, N. H., and G. M. Hewitt. 1985. Analysis of hybrid zones. Annu Rev Ecol Evol Syst 16:113–148.

Barton, N. H., and K. S. Gale. 1993. Genetic analysis of hybrid zones. In: Harrison R (ed) Hybrid zones and the evolutionary process, Oxford University Press, New York, pp 13–45.

Batalha-Filho, H., Cabanne, G. S., and C. Y. Miyaki. 2012. Phylogeography of an Atlantic Forest passerine reveals demographic stability through the last glacial maximum. Mol. Phylogenet. Evol. 65:892–902.

Behling, H. 1997. Late Quaternary vegetation, climate and fire history from the tropical mountain region of Morro de Itapeva, SE Brazil. Palaeogeogr. Palaeoclimatol. Palaeoecol. 129:407–422.

Behling, H. 2007. Late Quaternary vegetation, fire and climate dynamics of Serra do Araçatuba in the Atlantic coastal mountains of Paraná State, southern Brazil. Veg. Hist. Archaeobot. 16:77–85.

Behling, H., and V. D. Pillar. 2007. Late Quaternary vegetation, biodiversity and fire dynamics in the southern Brazilian highlands and their implications for conservation and management of modern *Araucaria* forest and grassland ecosystems. Philos. Trans. R. Soc. Lond. B. Biol. Sci. 362:243–251.

Behling, H., Dupont, L., DeForest Safford, H., and G. Wefer. 2007. Late Quaternary vegetation and climate dynamics in the Serra da Bocaina, southeastern Brazil. Quat. Int. 161:22–31.

Behling, H., Safford, H.D. 2010. Late-glacial and Holocene vegetation, climate and fire dynamics in the Serra dos Órgãos, Rio de Janeiro State, southeastern Brazil. Glob. Chang. Biol. 16:1661–1671.

Bolger, A. M., Lohse, M., and B. Usadel. 2014. Trimmomatic: a flexible trimmer for Illumina sequence data. Bioinformatics. 30:2114–2120.

Bonaccorso, E. 2009. Historical biogeography and speciation in the Neotropical highlands: molecular phylogenetics of the jay genus *Cyanolyca*. Mol Phylogenet Evol 50:618–632.

Brown, J. L., D. J. Hill, A. M. Dolan, A. C. Carnaval, and A. M. Haywood. 2018. PaleoClim, high spatial resolution paleoclimate surfaces for global land areas. Sci. Data 5:180254.

Cadena, C. D., K. H. Kozak, J. P. Gomez, J. L. Parra, C. M. McCain, R. C. K. Bowie, A. C. Carnaval, C. Moritz, C. Rahbek, T. E. Roberts, et al. 2012. Latitude, elevational climatic zonation and speciation in New World vertebrates.

Cadena, C. D., Pérez-Emán, J. L., Cuervo, A. M., Céspedes, L. N., Epperly, K. L., Klicka, J. T. 2019. Extreme genetic structure and dynamic range evolution in a montane passerine bird: implications for tropical diversification. Biol. J. Linnean Soc. 126:487–506.

Chesser, T. 2000. Evolution in the high Andes: the phylogenetics of *Muscisaxicola* Ground-Tyrants. Mol. Phylogenet. Evol. 15:369–380.

Cogné, N., Gallagher, K., Cobbold, P.R., Riccomini, C., and C. Gautheron. 2012. Post-breakup tectonics in southeast Brazil from thermochronological data and combined inverse-forward thermal history modeling. J. Geophys. Res. Solid Earth 117.

Csilléry, K., O. François, and M. G. B. Blum. 2012. abc: an R package for approximate Bayesian computation (ABC). Methods Ecol. Evol. 3:475–479.

Diazgranados, M., and J. C. Barber. 2017. Geography shapes the phylogeny of frailejones (Espeletiinae Cuatrec., Asteraceae): a remarkable example of recent rapid radiation in sky islands. PeerJ. https://doi.org/10.7717/peerj.2968. eCollection 2017.

De Marco Júnior, P., and C. C. Nóbrega. 2018. Evaluating collinearity effects on species distribution models: An approach based on virtual species simulation. PLoS One 13:e0202403.

Diniz-Filho, J. A. F., L. Mauricio Bini, T. Fernando Rangel, R. D. Loyola, C. Hof, D. Nogués-Bravo, and M. B. Araújo. 2009. Partitioning and mapping uncertainties in ensembles of forecasts of species turnover under climate change. Ecography (Cop.). 32:897–906.

Dormann, C. F., J. Elith, S. Bacher, C. Buchmann, G. Carl, G. Carré, J. R. G. Marquéz, B. Gruber, B. Lafourcade, P. J. Leitão, et al. 2013. Collinearity: a review of methods to deal with it and a simulation study evaluating their performance. Ecography (Cop.). 36:27–46. John Wiley & Sons, Ltd.

Faircloth, B. C., McCormack, J. E., Crawford, N. G., Harvey, M. G., Brumfield, R. T., and T. C. Glenn. 2012. Ultraconserved elements anchor thousands of genetic markers spanning multiple evolutionary timescales. Syst. Biol. 61:717–726.

Faircloth, B. C. 2014. Phyluce: phylogenetic estimation from ultraconserved elements. https://github.com/faircloth-lab/phyluce [WWW Document].

Faircloth, B. C. 2014. Illumiprocessor: a Trimmomatic wrapper for parallel adapter and quality trimming. https://github.com/faircloth-lab/illumiprocessor [WWW Document].

Fay, J. C., and C.-I. Wu. 2000. Hitchhiking under positive Darwinian selection. Genetics 155:1405 LP –1413.

Fjeldså, J., Bowie, R. C. K., and C. Rahbek. 2012 The role of mountain ranges in the diversification of birds. Annu. Rev. Ecol. Evol. Syst. 43:249–265.

Flantua, S. G. A., and H. Hooghiemstra. 2018. Historical connectivity and mountain biodiversity. In: C. Hoorn, A. Perrigo and A. Antonelli (Eds.). Mountains, Climate and Biodiversity, pp. 171–185. John Wiley & Sons.

Flantua, S. G. A., O'Dea, A., Onstein, R. E., Giraldo, C., and H. Hooghiemstra. 2019. The flickering connectivity system of the north Andean páramos. J. Biogeogr. 46:1808–1825.

Franco-Magalhães, A. O. B., Cuglieri, M. A. A., Hackspacher, P. C., and A. R. Saad. 2014. Long-term landscape evolution and post-rift reactivation in the southeastern Brazilian passive continental margin: Taubaté basin. Int. J. Earth Sci. 103:441–453.

Freeman, B. G., A. M. Class Freeman, and W. M. Hochachka. 2016. Asymmetric interspecific aggression in New Guinean songbirds that replace one another along an elevational gradient. Ibis 158:726–737.

Freitas, R. O. 1951. Relevos policíclicos na tectônica do escudo Brasileiro. Boletim Paulista Geociências 7:3–19.

Frichot, E., Mathieu, F., Trouillon, T., Bouchard, G., and O. François. 2014. Fast and efficient estimation of individual ancestry coefficients. Genetics 196:973–983.

Frichot, E., and O. François. 2015. LEA: An R package for landscape and ecological association studies. Methods Ecol. Evol. 6:925–929.

Galbreath, K. E., Hafner, D. J., Zamudio, K. R., Agnew, K., and M. Ebach. 2010. Isolation and introgression in the Intermountain West: contrasting gene genealogies reveal the complex biogeographic history of the American pika (*Ochotona princeps*). J. Biogeogr. 37:344–362.

Ghalambor, C. K., R. B. Huey, P. R. Martin, J. J. Tewksbury, and G. Wang. 2006. Are mountain passes higher in the tropics? Janzen's hypothesis revisited. Integr. Comp. Biol. 46:5–17.

Gehara, M., A. A. Garda, F. P. Werneck, E. F. Oliveira, E. M. da Fonseca, F. Camurugi, F. de M. Magalhães, F. M. Lanna, J. W. Sites, R. Marques, et al. 2017. Estimating synchronous demographic changes across populations using hABC and its application for a herpetological community from northeastern Brazil. Mol. Ecol. 26:4756–4771.

Golicher, D., A. Ford, L. Cayuela, and A. Newton. 2012. Pseudo-absences, pseudo-models and pseudo-niches: pitfalls of model selection based on the area under the curve. Int. J. Geogr. Inf. Sci. 26:2049–2063.

Graham, C. H., Carnaval, A. C., Cadena, C. D., Zamudio, K. R., Roberts, T. E., Parra, J. L., Mccain, C. M., Bowie, R. C. K., Moritz, C., Baines, S. B., et al. 2014. The origin and maintenance of montane diversity: Integrating evolutionary and ecological processes. Ecography 37:711–719.

Graves, G. R. 1988. Linearity of geographic range and its possible effect on the population structure of Andean birds. Auk 105:47–52.

Gutiérrez-Pinto, N., Cuervo, A. M., Miranda, J., Pérez-Emán, J. L., Brumfield, R. T., and C. D. Cadena. 2012. Non-monophyly and deep genetic differentiation across low-elevation barriers in a Neotropical montane bird (*Basileuterus tristriatus*; Aves: Parulidae). Mol. Phylogenet. Evol. 64:156–165.

Hackspacher, P. C., Ribeiro, L. F. B., Ribeiro, M. C. S., Fetter, A. H., Neto, J. C. H., Tello, C. E. S., and E. L. Dantas. 2004. Consolidation and breakup of the South American Platform in southeastern Brazil: Tectonothermal and denudation histories. Gondwana Res. 7:91–101.

Harvey, M. G., B. T. Smith, T. C. Glenn, B. C. Faircloth, and R. T. Brumfield. 2016. Sequence capture versus restriction site associated DNA sequencing for shallow systematics. Syst. Biol. 65:910–924.

Hewitt, G. M. 1996. Some genetic consequences of ice ages, and their role in divergence and speciation. Biol. J. Linnean Soc. 58:247–276.

Hewitt, G. M. 1999. Post-glacial re-colonization of European biota. Biol. J. Linnean Soc. 68:87–112.

Hijmans, R. J., Phillips, S., Leathwick, J., and J. Elith. 2017. dismo: Species Distribution Modeling. R package version 1.1-4. https://CRAN.R-project.org/package=dismo.

Hooghiemstra, H., and T. Van der Hammen. 2004. Quaternary Ice-Age dynamics in the Colombian Andes: developing an understanding of our legacy. Philos. Trans. R. Soc. Lond. B. Biol. Sci. 359:173–181.

Hudson, R. R. 2002. Generating samples under a Wright–Fisher neutral model of genetic variation. Bioinformatics 18:337–338.

Janzen, D. H. 1967. Why Mountain Passes are Higher in the Tropics. Am. Nat. 101:233.

Jaramillo, A. 2020a. Buff-throated Warbling-Finch (Microspingus lateralis), version 1.0. In: J. del Hoyo, A. Elliott, J. Sargatal, D. A. Christie, and E. de Juana (Eds.). Birds of the World. Cornell Lab of Ornithology, Ithaca, NY, USA. https://doi.org/10.2173/bow.rrwfin1.01

Jaramillo, A. 2020b. Gray-throated Warbling-Finch (Microspingus cabanisi), version 1.0. In: J. del Hoyo, A. Elliott, J. Sargatal, D. A. Christie, and E. de Juana (Eds.). Birds of the World. Cornell Lab of Ornithology, Ithaca, NY, USA. https://doi.org/10.2173/bow.gytwaf1.01

Jombart, T., Devillard, S., and F. Balloux. 2010. Discriminant analysis of principal components: a new method for the analysis of genetically structured populations. BMC Genet. 11:94.

Kadereit, J.W. 2015. The geography of hybrid speciation in plants. Taxon 64:673–687.

Karatzoglou, A., K. Hornik, A. Smola, and A. Zeileis. 2004. kernlab - An S4 package for kernel methods in R. J. Stat. Softw. 11.

Karger, D. N., Conrad, O., Böhner, J., Kawohl, T., Kreft, H., Soria-Auza, R. W., Zimmermann, N. E., Linder, H. P., and M. Kessler. 2017. Climatologies at high resolution for the earth's land surface areas. Scientific Data 4:170122.

Karl, M., Glasmacher, U. A., Kollenz, S., Franco-Magalhães, A. O. B., Stockli, D. F., and P. C. Hackspacher. 2013. Evolution of the South Atlantic passive continental margin in southern Brazil derived from zircon and apatite (U–Th–Sm)/He and fission-track data. Tectonophysics 604:224–244.

Kozak, K. H., and J. J. Wiens. 2007. Climatic zonation drives latitudinal variation in speciation mechanisms. Proc. R. Soc. B Biol. Sci. 274:2995–3003.

Kuhn, M. 2019. Package 'caret' - Classification and Regression Training.

Lawing, A. M., and P. D. Polly. 2011. Pleistocene climate, phylogeny, and climate envelope models: An integrative approach to better understand species' response to climate change. PLoS One 6:e28554.

Ledru, M.-P., Mourguiart, P., and C. Riccomini. 2009. Related changes in biodiversity, insolation and climate in the Atlantic rainforest since the last interglacial. Palaeogeogr. Palaeoclimatol. Palaeoecol. 271: 140–152.

Legendre, P., and Legendre, L. 1998. Numerical ecology. 2nd edition. Elsevier, Amsterdam.

Leigh, J. W., and D. Bryant. 2015. POPART: full-feature software for haplotype network construction. Methods Ecol. Evol. 6:1110–1116.

Li, H. 2013. Aligning sequence reads, clone sequences and assembly contigs with BWA-MEM. arXiv Prepr. arXiv1303.3997.

Lisiecki, L. E., and M. E. Raymo. 2005. A Pliocene-Pleistocene stack of 57 globally distributed benthic δ18O records. Paleoceanography 20:PA1003.

Manly BFJ. Multivariate Statistical Methods: A Primer. London: Chapman and Hall; 1994.

Manthey, J. D., Moyle, R. G., Gawin, D. F., Rahman, M. A., Ramji, M. F. S., and F. H. Sheldon. 2017. Genomic phylogeography of the endemic Mountain Black-eye of Borneo (*Chlorocharis emiliae*): montane and lowland populations differ in patterns of Pleistocene diversification. J. Biogeogr. 44:2272–2283.

Mayr, E., and J. M. Diamond. 1976. Birds on islands in the sky: Origin of the montane avifauna of Northern Melanesia. Proc. Natl. Acad. Sci. U. S. A. 73:1765–1769.

McCormack, J. E., Huang, H., and L. L. Knowles. 2009. Sky islands. Encycl. Islands 4:841–843.

McKenna, A., Hanna, M., Banks, E., Sivachenko, A., Cibulskis, K., Kernytsky, A., Garimella, K., Altshuler, D., Gabriel, S., Daly, M., et al. 2010. The genome analysis toolkit: A MapReduce framework for analyzing next-generation DNA sequencing data. Genome Res. 20:1297–1303.

Meisling, K. E., Cobbold, P. R., and V. S. Mount. 2001. Segmentation of an obliquely rifted margin, Campos and Santos basins, southeastern Brazil. AAPG Bulletin 85:1903–1924.

Melo, M. S., Riccomini, C., Hasui, Y., Almeida, F. F. M. A., and A. M. Coimbra 1985. Geologia e evolução do sistema de bacias tafrogênicas continentais do sudeste do Brasil. Rev. Bras. Geociências 15:193–201.

Minns, J., Buzzetti, D., Albano, C., Grosset, A., Whittaker, A., and R. Parrini. 2010. Aves Do Brasil, Vozes E Fotografias. V. 1 - Floresta Atlântica, Cerrado, Caatinga, Pantanal, Campos Sulinos E Costa. Versão 1.0 (Dvd-rom). Vinhedo, Avis Brasilis Editora.

Modenesi-Gauttieri, M.C., Takashi Hiruma, S., and C. Riccomini. 2002. Morphotectonics of a high plateau on the northwestern flank of the continental rift of southeastern Brazil. Geomorphology 43:257–271.

Moritz, C., J. L. Patton, C. J. Schneider, and T. B. Smith. 2000. Diversification of Rainforest Faunas: An Integrated Molecular Approach. Annu. Rev. Ecol. Syst. 31:533–563.

Muellner-Riehl, A. N. 2019. Mountains as Evolutionary Arenas: Patterns, Emerging Approaches, Paradigm Shifts, and Their Implications for Plant Phylogeographic Research in the Tibeto-Himalayan Region. Front. Plant Sci. https://doi.org/10.3389/fpls.2019.00195

Oliveira, M. A., Behling, H., and L. C. R. Pessenda. 2008. Late-Pleistocene and mid-Holocene environmental changes in highland valley head areas of Santa Catarina state, Southern Brazil. Journal of South American Earth Sciences 26:55–67.

Oliveira, M. A. T., Porsani, J. L., de Lima, G. L., Jeske-Pieruschka, V., and H. Behling. 2012. Upper Pleistocene to Holocene peatland evolution in Southern Brazilian highlands as depicted by radar stratigraphy, sedimentology and palynology. Quat. Res. 77:397–407.

Otto-Bliesner, B. L., S. J. Marshall, J. T. Overpeck, G. H. Miller, and A. Hu. 2006. Simulating Arctic Climate Warmth and Icefield Retreat in the Last Interglaciation. Science (80-.). 311:1751 LP –1753.

Patton, J. L., and M. F. Smith. 1992. mtDNA phylogeny of Andean mice: a test of diversification across ecological gradients. Evolution. 46:174–183.

Pavlidis, P., S. Laurent, and W. Stephan. 2010. msABC: a modification of Hudson's ms to facilitate multi-locus ABC analysis. Mol. Ecol. Resour. 10:723–727.

Pearson, R. G., C. J. Raxworthy, M. Nakamura, and A. Townsend Peterson. 2007. Predicting species distributions from small numbers of occurrence records: A test case using cryptic geckos in Madagascar. J. Biogeogr. 34:102–117.

Peres, E. A., Sobral-Souza, T., Perez, M. F., Bonatelli, I. A. S., Silva, D. P., Silva, M. J., and V. N. Solferini. 2015. Pleistocene niche stability and lineage diversification in the subtropical spider *Araneus omnicolor* (Araneidae). PLoS One 10:e0121543.

Peres, E. A., M. B. DaSilva, M. Antunes, and R. Pinto-Da-Rocha. 2018. A short-range endemic species from south-eastern Atlantic Rain Forest shows deep signature of historical events: phylogeography of harvestmen Acutisoma longipes (Arachnida: Opiliones). Syst. Biodivers. 16:171–187.

Peres, E. A., A. R. Benedetti, S. T. Hiruma, T. Sobral-Souza, and R. Pinto-da-Rocha. 2019. Phylogeography of Sodreaninae harvestmen (Arachnida: Opiliones: Gonyleptidae): Insights into the biogeography of the southern Brazilian Atlantic Forest. Mol. Phylogenet. Evol. 138:1–16.

Pérez-Emán, J. L. 2005. Molecular phylogenetics and biogeography of the Neotropical redstarts (*Myioborus*; Aves, Parulinae). Mol. Phylogenet. Evol. 37:511–528.

Pfeifer, B., U. Wittelsbürger, S. E. Ramos-Onsins, and M. J. Lercher. 2014. PopGenome: an efficient Swiss army knife for population genomic analyses in R. Mol. Biol. Evol. 31:1929–1936.

Pie, M. R., B. C. Faircloth, L. F. Ribeiro, M. R. Bornschein, and J. E. Mccormack. 2018. Phylogenomics of montane frogs of the Brazilian Atlantic Forest is consistent with isolation in sky islands followed by climatic stability. Biol. J. Linn. Soc. 125:72–82.

Pulido-Santacruz, P., Bornschein, M. R., Belmonte-Lopes, R., and S. L. Bonatto. 2016. Multiple evolutionary units and demographic stability during the last glacial maximum in the *Scytalopus speluncae* complex (Aves: Rhinocryptidae). Mol. Phylogenet. Evol. 102:86–96.

Rahbek, C., M. K. Borregaard, R. K. Colwell, B. Dalsgaard, B. G. Holt, N. Morueta-Holme, D. Nogues-Bravo, R. J. Whittaker, and J. Fjeldså. 2019. Humboldt's enigma: What causes global patterns of mountain biodiversity? Science Vol. 365:1108–1113.

Ramírez-Barahona, S., and L. E. Eguiarte. 2013. The role of glacial cycles in promoting genetic diversity in the Neotropics: the case of cloud forests during the Last Glacial Maximum. Ecol. Evol. 3:725–738.

Rangel, T. F., Edwards, N. R., Holden, P. B., Diniz-Filho, J. A. F., Gosling, W. D., Coelho, M. T. P., Cassemiro, F. A. S., Rahbek, C., and R. K. Colwell. 2018. Modeling the ecology and evolution of biodiversity: Biogeographical cradles, museums, and graves. Science 361:eaar5452.

Tajima, F. 1989. Statistical method for testing the neutral mutation hypothesis by DNA polymorphism. Genetics 123:585–595.

Tello Saenz, C. A., Hackspacher, P. C., Hadler Neto, J. C., Iunes, P. J., Guedes, S., Ribeiro, L. F. B., and S. R. Paulo. 2003. Recognition of Cretaceous, Paleocene, and Neogene tectonic reactivation through apatite fission-track analysis in Precambrian areas of southeast Brazil: association with the opening of the south Atlantic Ocean. J. South Am. Earth Sci. 15:765–774.

Slatkin, M. 1985. Rare alleles as indicators of gene flow. Evolution. 39:53–65.

Van der Hammen, T. 1961. The Quaternary climatic changes of northern South America. Ann. N. Y. Acad. Sci. 95:676–683.

Valderrama, E., Pérez-Emán, J. L., Brumfield, R. T., Cuervo, A. M., and C. C. Cadena. 2014. The influence of the complex topography and dynamic history of the montane Neotropics on the evolutionary differentiation of a cloud forest bird (*Premnoplex brunnescens*). J.Biogeogr. 41:1533–1546.

Watterson, G. A. 1975. On the number of segregating sites in genetical models without recombination. Theor. Popul. Biol. 7:256–276.

Wiens, J. J. 2004. Speciation and ecology revisited: pylogenetic niche conservatism and the origin of species. Evolution 58:193–197.

Weir, J. T. 2009. Implications of genetic differentiation in Neotropical montane forest birds. Annals of the Missouri Botanical Garden. 96:410–433.

Winger, B. M. 2017. Consequences of divergence and introgression for speciation in Andean cloud forest birds. Evolution. 71: 1815–1831.

Winger, B. M., and J. M. Bates. 2015. The tempo of trait divergence in geographic isolation: Avian speciation across the Marañon Valley of Peru. Evolution 69:772–787.

Wright, S. 1949. The genetical structure of populations. Ann. Eugen. 15:323–354. John Wiley & Sons, Ltd.

Zamudio, K. R., Bell, R. C., and N. A. Mason. 2016. Phenotypes in phylogeography: Species' traits, environmental variation, and vertebrate diversification. Proc. Natl. Acad. Sci. U. S. A. 113:8041–8.

Zuur, A. F., E. N. Ieno, and C. S. Elphick. 2010. A protocol for data exploration to avoid common statistical problems. Methods Ecol. Evol. 1:3–14.

Associate Editor: J. A. Tobias
Handling Editor: A. G. McAdam

Supporting Information

Additional supporting information may be found online in the Supporting Information section at the end of the article.

Figure S1. Cross-entropy sNMF runs for alpha values of 1, 10, 100 and 1,000.

Figure S2. BIC values of (a) K-clustering method and (b) DAPC plot for two populations.

Figure S3. Principal Component Analysis of the six simulated models for the topology test, and observed data for the *Microspingus* populations.

Table S1. Samples used in the present study.

Table S2. Coefficients from smooth terms and interactions in the full Generalized Additive Mixed Model - GAMM ($R^2 = 0.73$).

Table S3. Cross-validation predicted error for estimated demographic parameters for three distinct tolerance levels, 0.001 (1,000 simulations), 0.01 (10,000 simulations) and 0.05 (50,000 simulations). Ne - effective population size; Tdiv 1 - the divergence between *Microspingus lateralis* and Caparaó; Tdiv 2 - the divergence between *M. cabanisi* and *M. lateralis*+Caparaó; mig cab → lat - migration from *M. cabanisi* to *M. lateralis*; mig lat → cab - migration from *M. lateralis* to *M. cabanisi*; μ - mutation rate.

Table S4. Pearson's correlation index between simulated and pseudo-observed data under the best demographic model [m1_23 - (*M. cabanisi*, (*M. lateralis*, Caparaó)) without population size change], assuming a tolerance level of 0.001 (1000 simulations). Ne - effective population size; Tdiv 1 - the divergence between *Microspingus lateralis* and Caparaó; Tdiv 2 - the divergence between *M. cabanisi* and *M. lateralis*+Caparaó; mig cab → lat - migration from *M. cabanisi* to *M. lateralis*; mig lat → cab - migration from *M. lateralis* to *M. cabanisi*; μ - mutation rate.

Supporting information